An experimental study of a turbulent shear layer at a clean and contaminated free-surface

Amy Warncke Lang, Carlos E. Manglano

Abstract An experimental study was performed to measure the flow properties of a vertically-oriented shear layer in the vicinity of a free-surface. The effect of surface contamination on the near surface flow field was also determined. Digital Particle Image Velocimetry was used to measure instantaneous and averaged velocity, vorticity, and Reynolds stresses. Results show that the presence of surfactants can cause directional shifts of the shear layer, as well as an overall damping of the turbulence in the vicinity of the free-surface, except in the vicinity of a Reynolds ridge where an increase in Reynolds stress was observed.

Keywords Turbulent shear layer, Surfactants, Free-surface

1
Introduction

The study of surfactants on free-surface phenomena has ranged from understanding their effects on wave damping to two-phase flows. However, observations of their effects on turbulent flows at a free-surface has been limited. Davies (1966) was one of the first to notice the damping of turbulent eddies at a free-surface by the presence of surfactants. One of the more recent studies is that of Tsai (1996), who computationally looked at the presence of turbulence at a free-surface due to a wind-blown interface. The turbulence in this simulation was composed of the flow field associated with a wall-bounded shear flow (containing horseshoe or hairpin structures). In the con-

A. W. Lang (✉), C. E. Manglano
Department of Aerospace and Mechanical Engineering,
Parks College of Engineering and Aviation,
Saint Louis University,
3450 Lindell Blvd.St. Louis, MO63103, USA
E-mail: langaw@slu.edu

taminated surface case, Tsai found an overall damping in the turbulent intensities for all three components when compared to a clean one. Another recent study by Milgram (1998) focused on short wave damping in the presence of both surfactants and sub-surface grid-generated turbulence.

In addition, a study by Hirsa et al. (1995) looked at the decay of a columnar vortex attached normally to a free-surface in the presence of both a clean and surfactant coated surface. They found that the contaminated case showed a disconnection and therefore earlier vortex breakdown in the vicinity of the free-surface. Finally, Lang and Gharib (2000) showed that the connection process of vortices shed from the wake of a cylinder in a low Reynolds number flow near the free-surface was significantly altered by the presence of surfactants. In fact it was shown that these vertically-oriented vortices, which connect normally to a clean free-surface, would in fact pair up and form a vortex connection below and parallel to the free-surface.

The presence of a clean free-surface on a turbulent flow field is one that has received much study in recent years. One of the more recent studies was that by Shen et al. (1999) where they described two kinds of layers associated with free-surface turbulence. The first is a thicker "source" or "blockage" layer, which, due to the kinematic boundary condition of a free-surface reducing vertical fluctuations, shows a redistribution of the turbulence intensity with an increase in horizontal velocity fluctuations. This layer typically has a size of the order of the characteristic macro length scale of the flow. The second layer is defined at the "surface layer" in which the magnitudes of both horizontal components of vorticity, as well as the gradient in vertical vorticity, are reduced. For high Reynolds number flow this layer is much thinner, typically of the order of a few millimeters, and is due to the dynamic zero-stress boundary condition at a clean free-surface.

However in this study, a shear layer, oriented vertically to the free-surface, was used to study the effect of surfactants on the turbulent properties and their variations between that of the bulk fluid, clean surface, and contaminated surface. In this case, the turbulent eddies have a more coherent structure to them than that found in general homogenous or even wall-bounded turbulence. Larger coherent structures are known to form in the free shear layer, and in this case are oriented vertically to the free-surface. The clean surface case of this shear layer was first studied at a higher Reynolds number by Maheo (1998). He observed a slight directional shift in the shear layer to the

high-speed side in the vicinity of the free-surface. This was attributed to the greater strength of the on-average surface-parallel vortex forming on the high-speed side in the vicinity of the free-surface. The presence of this on-average vortex pair also caused a smaller growth rate for the shear layer in a small region below the free-surface. This is due to a region of flow convergence created by the on-average vortex pair. Now, the presence of the free-surface with surfactants will locally create surface tension gradients due to the turbulence that will generate regions of high and low surfactant concentrations, and these result in shear stresses at the free-surface.

Results show that the presence of surfactants tends to damp turbulence in the free-surface plane, which is in agreement with observations by other researchers. However, turbulent structures in the vicinity of a Reynolds ridge, where a sudden drop in surface tension occurs, have been found to lead to localized increases in surface Reynolds stresses. Also, an additional directional shift in the shear layer was observed in the vicinity of the free-surface, and is presumed to be due to the overall surface tension gradient formed within the test section.

From a wider point of view, this type of experiment can give a better understanding of the flows found in ship wakes, where naturally occurring surfactants abound at the ocean surface, and concentrated bands of surfactants are known to form within the wake (Reed and Milgram 2002).

2
Theory
To understand the behavior of turbulence at a free-surface, one must first understand the behavior of vortex structures in the vicinity of various boundaries. The boundary conditions for the case of a flat free-surface, depending on the adjoining medium, are described by Gharib and Weigand (1996). In the case of a clean (and so shear-free) surface, they show that only the surface-normal component of vorticity is allowed to exist at the surface. This leads to the formation of the "surface" layer. In the case of a stationary solid surface, due to the no-slip condition at the wall, only surface-parallel vorticity can exist at the surface. Therefore, for clean surfaces, vortex filaments will connect normally to a free-surface. However in the case of the solid boundary, disconnected filaments cannot attach normally at the boundary and will connect with nearby vorticity of the same rotation and/or lead to the formation of a horseshoe or toroidal vortex.

For the case of surfactants present on a surface, the shear-free stress condition no longer applies at the water surface. Accounting for possible stresses due to any movement of air above the surface, as well as that from the presence of surfactants, the free-surface boundary condition is written as (with s as the surface-parallel coordinate):

$$\tau_{rs} = \tau_{AIR} + \frac{\partial \sigma}{\partial s} + (\kappa^s + \mu^s) \frac{\partial^2 u_s}{\partial s^2} \qquad (1)$$

where this equation was presented in whole by Lang and Gharib (2000) and used by Edwards et al. (1991) to derive

the last term containing the dilitational (κ^s) and shear (μ^s) viscosities of the surfactant film. One can see that larger surface viscosities can cause larger shear stresses and damp turbulent fluctuations in the free-surface plane. It also allows for the fact that even in the flat free-surface case, all components of vorticity may persist at a contaminated surface. It should also be noted that shear stresses at a free-surface can lead to surface tension gradients and vice versa.

In this particular case, a surface tension gradient is fabricated across a shear layer, and according to the above equation the net effect will be a shear stress imposed on the flow at the free-surface. The impact of this shear stress on the free-surface velocity, vorticity and Reynolds stress fields was measured, along with any local damping of the turbulence by the presence of the free-surface and surfactants.

3
Experiment
A small water tunnel facility similar to the one used by Lang and Gharib (2000), with a test section of 12 inches wide by 6 inches deep by 30 inches long was utilized. The width of this facility was chosen so that boundary layer effects from the test section walls would be minimal. This facility has been fabricated to have two separate free stream flows, allowing for a shear layer aligned normally to the free-surface with the use of a splitter plate. The velocity of the two streams were run for two test conditions. The first case was run at 24 and 12 cm/s. However, capturing the free-surface plane was difficult due to higher surface deformations. Therefore, a lower velocity case was repeated for 21 and 9 cm/s, retaining the same difference of 12 cm/s between the two streams.

The resulting thickness of the shear layer had a value $\delta = 4$ cm on average over the region studied. This corresponds to a Reynolds number of 4800, based on ΔU and δ. The contamination of the free-surface was achieved through the use of a surface barrier, which stopped the surfactant from continuing downstream with the flow and getting mixed with the bulk fluid. The surfactant used for this study was SDS (Sodium Dodecyl Sulfate), a common soluble surfactant found in other studies (Lang and Gharib 2000). This created a region of high concentration in SDS, and lead to the formation of a Reynolds ridge (Scott 1982). This Reynolds ridge, which took the shape of the velocity profile across the shear layer, created a surface tension gradient perpendicular to the flow direction at the free-surface (see Fig. 1). Knowing the surface properties of SDS (Chang and Frances 1995), this lead to an approximate drop in surface tension across the ridge assumed to be of the order of 5–15 mN/m. Note also that a greater change in surface tension would occur across the ridge on the high-speed side due to a greater compression of the surface film in this vicinity. In addition, the shape of the ridge also allowed for a surface tension gradient to exist across the test section, with a higher on-average surface tension located on the high-speed side. Any surfactant effects upstream of the location of the ridge are considered negligible. This is presumed due to the fact that vortex structures have been observed upstream of a Reynolds
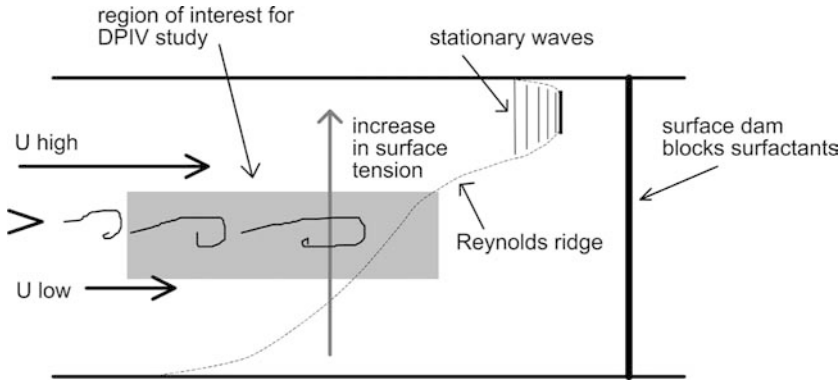
386

ridge unchanged from that of the clean surface case, in both this study and Lang and Gharib (2000). This is true because the concentration of surfactant upstream of the ridge is so minimal that no changes in surface tension would occur upstream of the ridge.

A Digital Particle Image Velocimetry (DPIV) system was used to capture two-dimensional velocity fields at various planes parallel and normal to the free-surface. The DPIV system used the software package PIXELFLOW, which is based on a program initially developed by Willert and Gharib (1991), and a 25 mJ Nd-Yag laser. The experiment was performed by studying several planes at different depths for both cases (with and without surfactant) on the water surface. This was done in order to detect the depth to which the surface conditions affected the bulk fluid flow. Then measurements of the turbulent quantities, such as Reynolds stress ($<u'v'>$), and averaged flow fields were obtained by averaging numerous (5,000 or more) velocity fields. Lastly, a shadowgraph system was used to view a six inch area of the free-surface so as to observe various instantaneous vortical structures interacting at the different surface conditions.

4
Results
The first case performed had freestream speeds of 24 and 12 cm/s for the high and low speed sides respectively.

Fig. 2 shows the averaged vorticity for the bulk fluid, taken at a depth of 5 cm. It also shows the same plot for the clean free-surface case, taken at a depth of 0.75 cm below the free-surface. At 0.75 cm depth, an opposite trend to that expected was observed, in that a decrease in shear layer growth was observed near the free-surface when compared to the bulk case (see Fig. 3). The growth rate of the shear layer is compared to a theoretical value based on the formula:

$$\delta = \alpha \left(\frac{1-r}{1+r} \right) x \qquad (2)$$

This formula is derived from Dimotakis (1986), where δ is the shear layer thickness, r is the freestream velocity ratio, x is the downstream distance from the splitter plate edge, and α is an empirical constant typically found to be in the range of $0.16 < \alpha < 0.18$. Here δ is based on the definition where the velocity meets 99% of the freestream value. It should also be noted that at $x=0$ the experimental shear layer thickness does not approach zero. This is due to the fact that the boundary layers generated off either side of the splitter plate meet to form a wake, so an initial thickness is given to the shear layer due to the presence of this wake. One can also observe that the experimental shear layer appears to have a slightly larger slope, or growth rate, than that proposed by the theory.
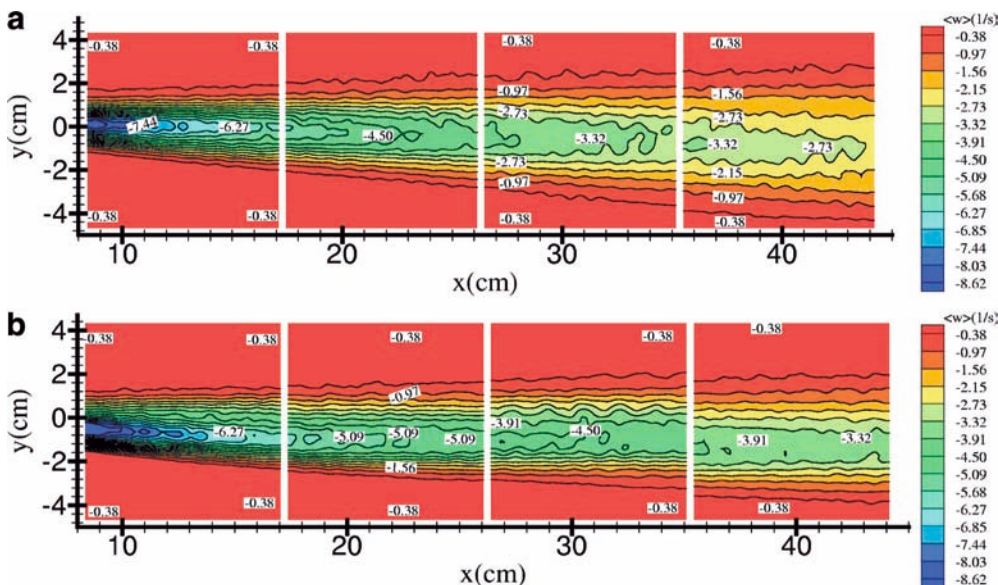

Fig. 2. a Clean and **b** bulk average vorticity contour plots for the case of 24 and 12 cm/s for the high and low speed streams respectively. Clean case taken at a depth of 0.75 cm and bulk at a depth of 5 cm
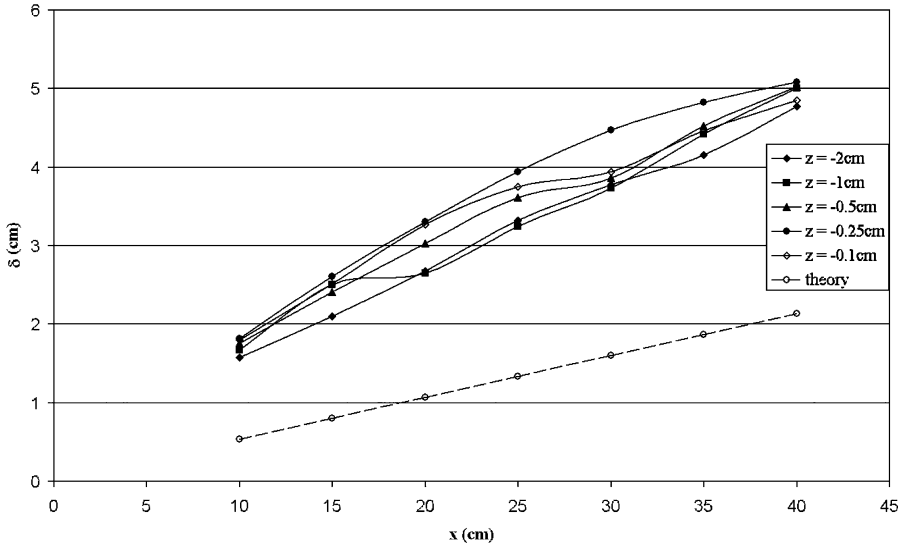
Fig. 3. Shear layer thickness (δ) plotted versus downstream distance from the splitter plate

It was also observed that the contaminated surface case showed a slightly larger growth rate on average than the clean surface case, but still lower than the bulk. Due to the smaller shear layer thickness, the vorticity in the free-surface case was greater than for the bulk. However, a pulling of the shear layer to the high-speed side was observed in the vicinity of the free-surface, consistent with previous observations. Next, the Reynolds stress ($<u'v'>$) data for this case is shown in Fig. 4 for the bulk and clean surfaces. An increase in Reynolds stress at the 0.75 cm depth is observed for the clean case over the bulk fluid. This is consistent with the "blockage" layer theory and previous researchers.

Due to the higher velocity values used in the above case, it was hard to obtain images close to the free-surface with the laser sheet, because of surface deformations. As a result, a lower velocity case was run at 21 and 9 cm/s for the high- and low-speed sides of the shear layer respectively. Since the higher speed of 21 cm/s is less than the critical value for standing waves to be generated from the presence of the Reynolds ridge, surface deformations were much lower. As a result, DPIV data was acquired within 0.1 cm of the free-surface for the clean and contaminated cases, and data for these two cases will be compared for these experimental conditions. The presence of the ridge is obvious, as shown in Fig. 5 where velocity profiles for the contaminated case are shown at various downstream positions ($x=0$ cm indicates the end of the splitter plate). It should be noted that the low-speed side is affected at earlier downstream distances due to the position of the ridge moving further upstream on the low-speed side, as depicted in Fig. 1. Also, negative values at the surface were measured, indicating that a backflow was occurring in the monolayer within this region of the test section.

Averaged vorticity plots for the previous case are shown in Fig. 6 for the clean and contaminated free-surface taken at a depth of 0.1 cm. The placement of the ridge is observable by an increase in vorticity magnitude and change in orientation of the contours, consistent with positioning of the ridge across the shear layer. A widening
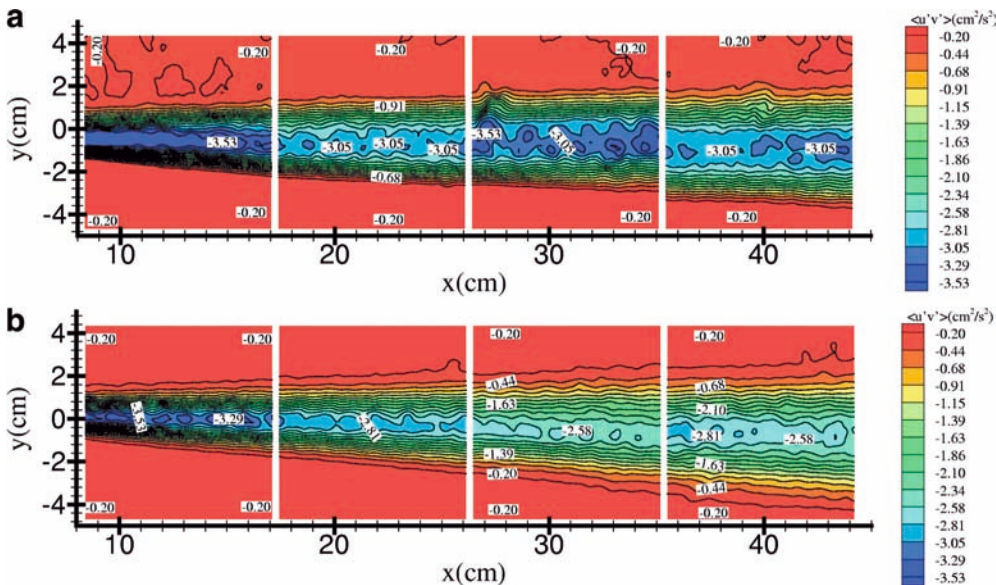

Fig. 4. a Clean and **b** bulk Reynolds stress contours for the case of 24 and 12 cm/s for the high and low speed streams respectively. Clean case taken at a depth of 0.75 cm and bulk at a depth of 5 cm
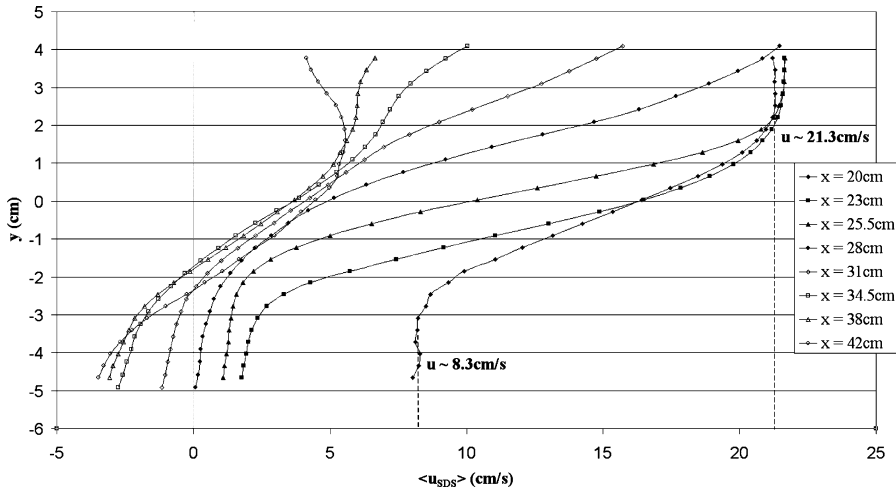
Fig. 5. Velocity profiles at a depth of 0.1 cm for the contaminated surface case, located at various downstream distances from the splitter plate

388

of the shear layer upon meeting and crossing through the ridge is also visible. In addition, the shear layer is pulled further towards the high-speed side when compared to the clean surface case. Fig. 7 shows the corresponding Reynolds stress contours. Immediately it is apparent that there is a dramatic increase in Reynolds stress associated with the shear layer passing through the ridge. However, consistent with previous observations, ahead of the ridge there is a damping of the turbulent fluctuations compared to the clean case, due to the presence of ambient surfactants, even ahead of the ridge. Even though a monolayer is only present behind the ridge, a surface tension gradient was set up across the test section, as pictured in Fig. 1.

Fig. 8 shows the Reynolds stress peak values as a function of downstream distance, and it is apparent that the peak value more than quadruples within the region of

the ridge, compared to the clean case. This localized area of increased velocity fluctuations can be attributed to the restoring force of the monolayer. A free-surface instantaneous vorticity contour plot is given in Fig. 9a, and a schematic of what is occurring in this flow field through the ridge is shown in Fig. 9b. The light gray line shows the equilibrium position of the ridge, which follows the average velocity profile of the shear layer. However, the shear layer is composed of turbulent coherent structures. As these structures interact with the ridge, they have the tendency, on an instantaneous basis, to deflect the ridge and elongate it. However, the ridge tries to restore itself to its equilibrium position, and because of the elasticity of the film, due to regions of higher surface tension created by expanding and stretching the monolayer, the presence of the Reynolds ridge induces additional surface velocity
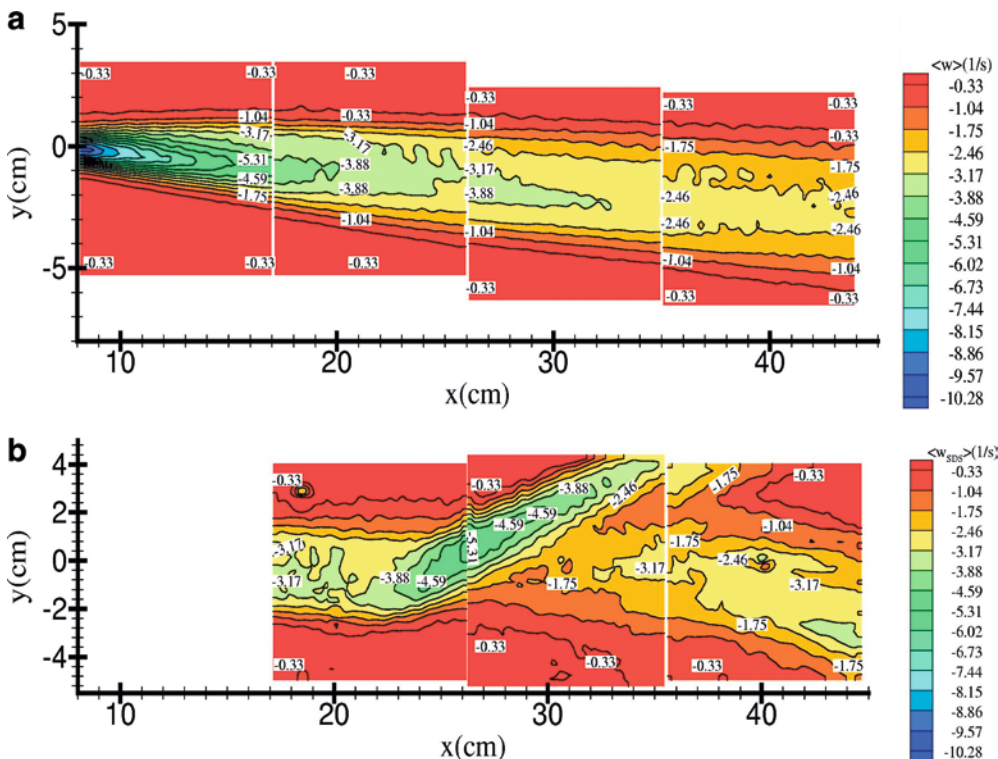

Fig. 6. a Clean and **b** contaminated average vorticity contour plots for the case of 21 and 9 cm/s for high and low speed streams respectively. Both taken at a depth of 0.1 cm
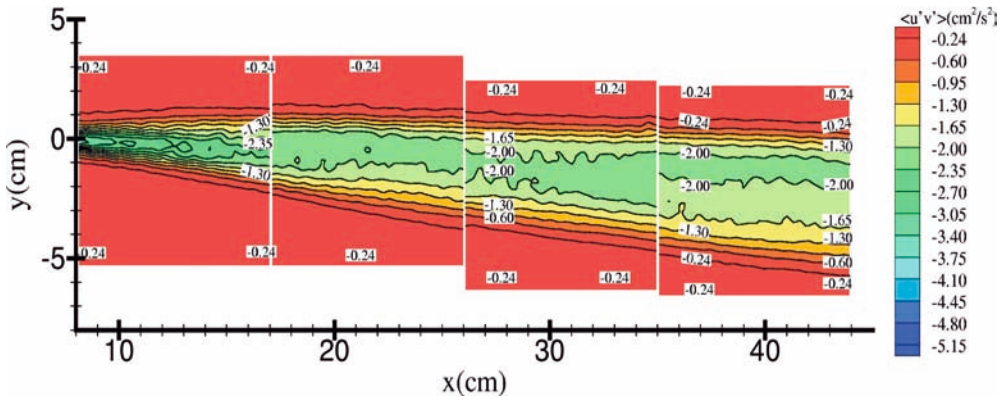
Fig. 7. a Clean and **b** contaminated Reynolds stress contour plots for the case of 21 and 9 cm/s for high and low speed streams respectively. Both taken at a depth of 0.1 cm

fluctuations. It would be interesting to repeat the experiment to observe whether monolayers with varying elasticities generate different magnitudes of Reynolds stress values in the vicinity of the ridge. Also note in Fig. 7b a region after the ridge where the Reynolds stress is negligible, but then beyond that a large region of Reynolds stress comparable in magnitude to levels previously observed in the clean case. Here it appears the presence of the monolayer has begun to stretch the vortex structures, as seen in Fig. 9a, and the stronger structures come back and interact at the surface, leading to this region of observed Reynolds stress.

A plot of shear layer thickness comparing the clean and contaminated cases at various depths is shown in Fig. 10. As stated previously, the contaminated cases show a greater growth rate compared to the clean cases. A pictorial explanation of the shear layer growth rates observed in this study is given in Fig. 11. Due to the presence of the on-average coherent vortex structures, which are generated due to the shear layer interacting at a free-surface, a decrease in shear layer growth is expected at a certain depth below the surface where the vortex pair creates a converging flow on average. In this case, the decrease in

shear layer growth was observed around a depth of 0.75 cm. Also, for a shear layer, the vortex structure generated on the high-speed side is of greater magnitude. This results in a slight pulling of the clean free-surface shear layer to the high-speed side. The additional pull observed for the contaminated case is attributed to the surface tension gradient formed across the shear layer, with the cleaner surface (high surface tension) pulling the shear layer on the high-speed side. Finally, there is a widening of the shear layer at the surface again due to the on-average flow induced by the counter-rotating vortex pair.

It should be noted that DPIV data was acquired in planes vertical to the free-surface and parallel to the flow. However, due to the shift in the shear layer position, it was not possible to obtain a plane that cut at all times through the center of the shear layer. Therefore DPIV results showed a velocity gradient with depth through these cuts, as the plane would cut through the center of the shear layer at the surface, but at lower depths of a few centimeters, a higher free stream flow would be measured. However, a reduction in vertical velocity fluctuations was measured within a region of 1 cm of the free-surface, consistent again with "blockage" layer theory.
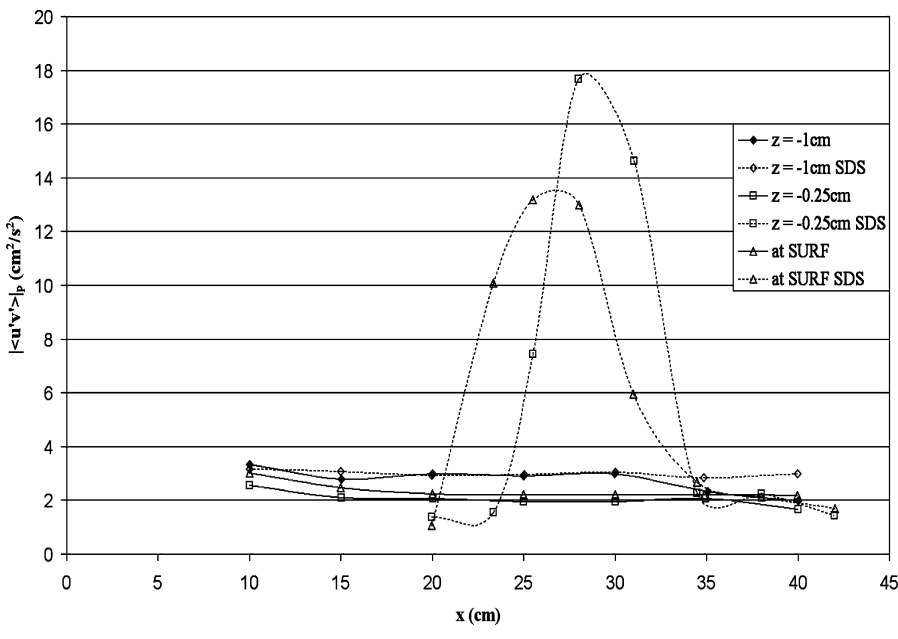

Fig. 8. Progression of Reynolds stress peak values plotted versus downstream distance for various depths and clean and contaminated (SDS) surface conditions
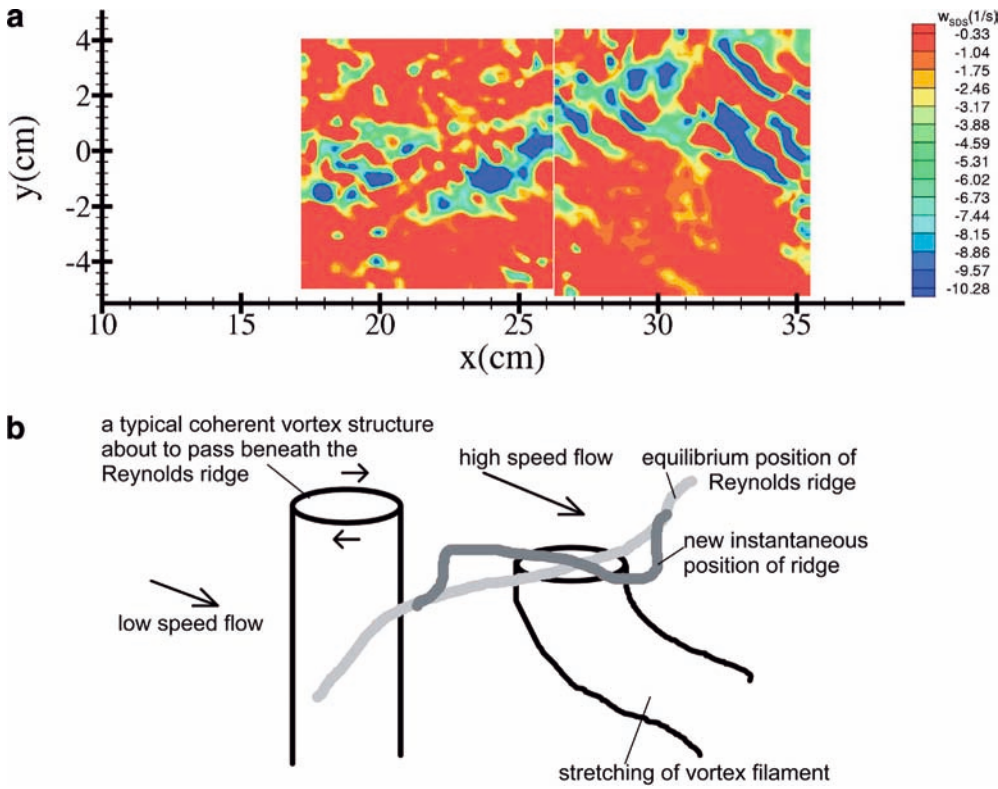
Fig. 9. a Instantaneous vorticity fields taken at a depth of 0.1 cm showing the elongation of vortex filaments as they pass through the Reynolds ridge. **b** A schematic of a typical coherent structure formed in the shear layer passing beneath the Reynolds ridge. The new instantaneous position of the ridge generates a restoring force in the monolayer to bring the ridge back to its equilibrium position

Lastly, shadowgraph images of the free-surface for the clean and contaminated surface conditions were acquired. Sequential image pairs showing the behavior of particular vortex structures observed in this flow field are shown in Figures 12, 13, 14 and 15. A region approximately 13 cm wide was observed. Flow is from left to right, and the high-speed flow is located on the bottom of the images. The higher speed case, with freestream velocities of 24 and 12 cm/s, was run for the shadowgraph experiment.

Figures 12 and 13 are located in the flow upstream of the position of the ridge, showing the structures in the shear layer through a region of approximately 5 to 18 cm downstream of the splitter plate. For the clean case, an amalgamation of vortex structures connected to the free-surface can be observed. This process of amalgamation is known to occur in the typical growth process of a free shear layer (Dimotakis 1986). However for the contaminated case, a disconnection or damping of weaker structures can be observed, while stronger structures remain attached to the surface.

Figures 14 and 15 image a region located approximately 21 to 34 cm downstream of the splitter plate. As a result, the Reynolds ridge is observed as the bright white line moving diagonally across the bottom of the image in Fig. 15. In addition, the standing waves generated from the ridge are observed on the high-speed side. Again, for the
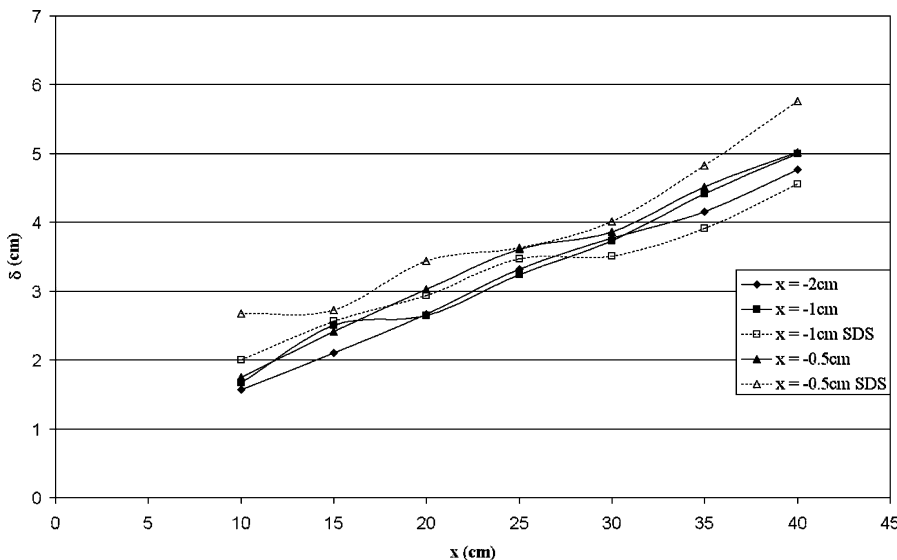

Fig. 10. Shear layer thickness (δ) plotted versus downstream distance at various depths and clean and contaminated (SDS) surface conditions
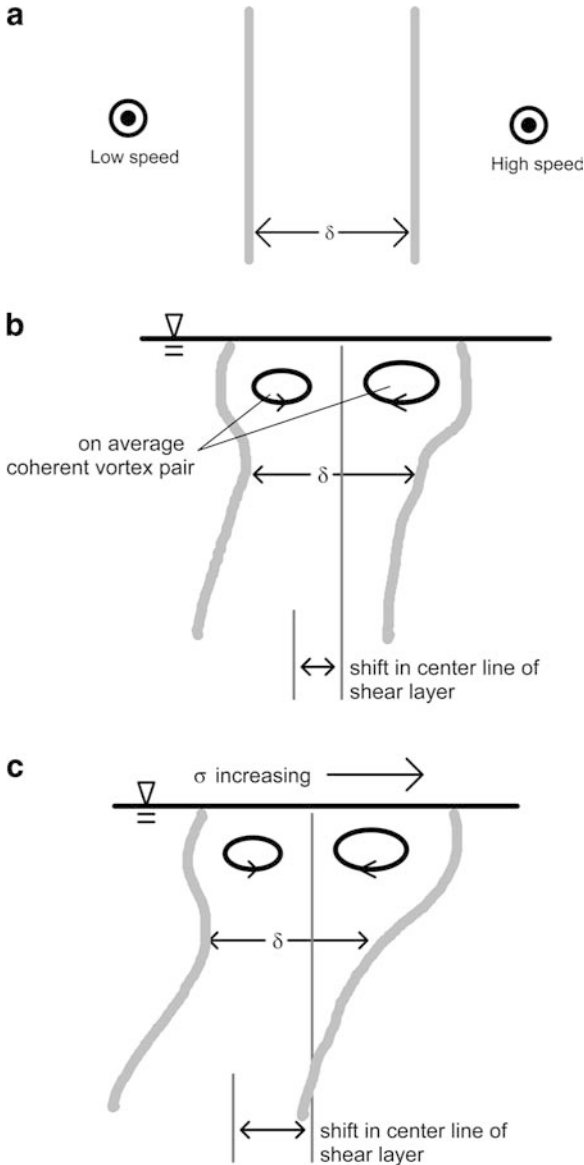
Fig. 11. A schematic of shear layer thickness depicted at a downstream distance of 15 cm from the splitter plate as viewed from looking downstream (flow out of the page) for **a** bulk fluid, **b** clean surface and **c** contaminated surface conditions
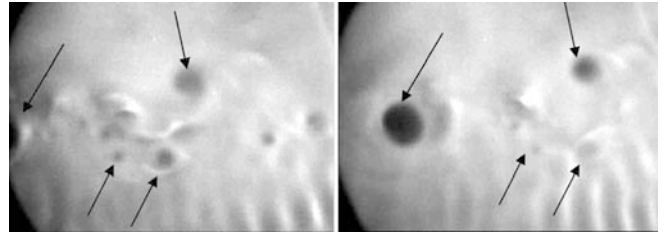
Fig. 13. Shadowgraph image pair from same region as in Fig. 12 but with a contaminated free-surface. Top arrows indicate a strong structure staying normally connected to the surface. Bottom arrows indicate weaker structures have surface-normal connection disappearing

the ridge, some disconnection of weaker vortex structures is observed. However, a stronger vortex structure appears to have been stretched, and approached the surface with a surface parallel orientation. This is due to the combined effects of passing through the ridge and the presence of a boundary layer formed beneath the monolayer, behind the Reynolds ridge. The boundary layer, first measured using DPIV by Warncke et al. (1996), is similar in nature to that formed on a flat plate, and so it generates a thin region of high shear near the free-surface. However, it should be noted that the boundary layer did not prevent the vortex structure from coming up and interacting at the free-surface.

5
Conclusions

This experimental study confirmed several previous observations about the nature of turbulent flows at a free-surface. First, damping of the vertical velocity fluctuations, and an increase in surface-parallel velocity fluctuations were observed, consistent with "blockage" layer theory. Secondly, observations of shear layer growth and directional shift at a clean free-surface were consistent with previous results. But, in addition, a larger growth rate of the shear layer was observed for the contaminated case. Also, a damping of surface-parallel fluctuations was observed upstream of the Reynolds ridge, consistent with previous research and theory.

However, a dramatic increase in local Reynolds stress was observed in the vicinity where the shear layer passes through a Reynolds ridge. These new results, at first glance, appear to contradict the hypothesis that the presence of surfactants have the tendency to damp turbulence

clean case in Fig. 14, the sequential images show the amalgamation of vortex structures into a larger coherent structure. Also, smaller vortex structures were found to stay attached to the surface. In Fig. 15, with the presence of
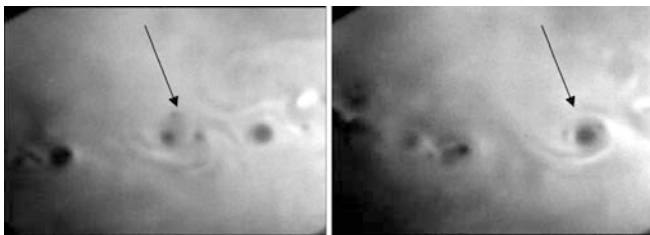

Fig. 12. Shadowgraph image pair of a shear layer at a clean free-surface showing a region approximately 5 to 18 cm downstream of the splitter plate. Arrows indicate a vortex pairing
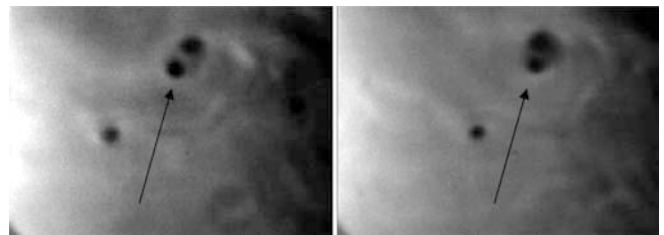

Fig. 14. Shadowgraph image pair of a shear layer at a clean free-surface showing a region approximately 21 to 34 cm downstream of the splitter plate. Arrows indicate a vortex pairing
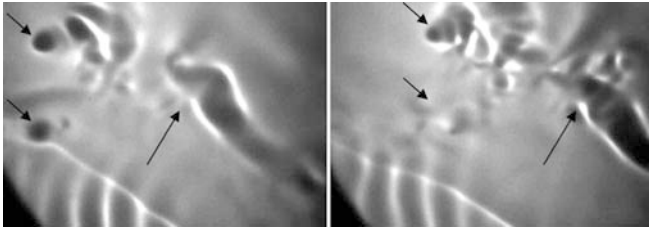
Fig. 15. Shadowgraph image pair from same region in Fig. 14, but with a contaminated free-surface. Reynolds ridge observed in bottom right of images as bright diagonal line. Left arrows indicate surface-normal connection disappearing. Right arrows indicate surface-parallel structure coming up to the surface

392

and surface waves. However, upon review of the results, one can deduce that at this critical juncture, where the turbulent flow enters a surface covered by a surfactant monolayer, the restoring force of the monolayer causes additional instantaneous surface velocity fluctuations. A stretching and twisting of vortex filaments to the surface-parallel direction through this region was also observed. Therefore, the increase in Reynolds stress is associated with the interaction of the Reynolds ridge with the coherent vortex structures produced by the shear layer.

References

Chang C, Frances E (1995) Adsorption dynamics of surfactants at the air/water interface: a critical review of mathematical models, data, and mechanisms. Colloids Surf, A 100:1–45

Davies JT (1966) The effects of surface films in damping eddies at a free-surface of a turbulent liquid. P Roy Soc Lond A Mat 290:515–526

Dimotakis P (1986) Two-dimensional shear layer entrainment. AIAA J 24(11):1791–1796

Edwards D, Brenner H, Wasan D (1991) Interfacial transport processes and rheology. Butterworth-Heinemann, Stoneham, MA

Gharib M, Weigand A (1996) Experimental studies of vortex disconnection at a free-surface. J Fluid Mech 321:59–86

Hirsa A, Harper J, Kim S (1995) Columnar vortex generation and interaction with a clean and contaminated free-surface. Phys Fluids 11:2532–2534

Lang AW, Gharib M (2000) Experimental study of the wake behind a surface-piercing cylinder for a clean and contaminated free-surface. J Fluid Mech 402:109–136

Maheo P (1998) Free-surface turbulent shear flows. PhD Thesis, California Institute of Technology, CA

Milgram J (1998) Short wave damping in the simultaneous presence of a surface film and turbulence. J Geophys Res 103(C8):15,717–15,727

Reed A, Milgram J (2002) Ship wakes and their radar images. Annu Rev Fluid Mech 34:469–502

Scott J (1982) Flow beneath a stagnant film on water: the Reynolds ridge. J Fluid Mech 116:283–296

Shen L, Zhang X, Yue D, Triantafyllou G (1999) The surface layer for free-surface turbulent flows. J Fluid Mech 386:167–212

Tsai W (1996) Impact of a surfactant on a turbulent shear layer under the air-sea interface. J Geophys Res 101(C12):28,557–28,568

Warncke A, Gharib M, Roesgen T (1996) Flow measurements near a Reynolds ridge. J Fluids Eng 118:621–624

Willert C, Gharib M (1991) Digital particle image velocimetry. Exp Fluids 10:181–193